Biogeosciences Discuss., 11, 17925–17965, 2014
www.biogeosciences-discuss.net/11/17925/2014/
doi:10.5194/bgd-11-17925-2014

Biogeosciences Discussions
Open Access

Glacial meltwater and primary production as drivers for strong CO_2 uptake in fjord and coastal waters adjacent to the Greenland Ice Sheet

L. Meire[1,2,3], D. H. Søgaard[1], J. Mortensen[1], F. J. R. Meysman[2,4], K. Soetaert[2], K. E. Arendt[1], T. Juul-Pedersen[1], and S. Rysgaard[1,5,6,7]

[1]Greenland Institute of Natural Resources, Greenland Climate Research Centre, P.O. Box 570, Kivioq 5, 3900 Nuuk, Greenland
[2]Royal Netherlands Institute of Sea Research (NIOZ), Department of Ecosystem Studies, Korringaweg 7, 4401, Yerseke, the Netherlands
[3]University of Ghent (UGent), Marine Biology Laboratory, Krijgslaan 281 (S8), 9000 Gent, Belgium
[4]Department of Analytical, Environmental and Geochemistry, Vrije Universiteit Brussel (VUB), Pleinlaan 2, 1050 Brussel, Belgium
[5]Centre for Earth Observation Science, Department of environment and Geography, University of Manitoba, Winnipeg, MB R3T 2N2, Canada
[6]Department of Geological Sciences, University of Manitoba, Winnipeg, MB R3T 2N2, Canada
[7]Arctic Research Centre, Aarhus University, 8000 Aarhus, Denmark

Received: 26 November 2014 – Accepted: 1 December 2014 – Published: 19 December 2014

Correspondence to: L. Meire (lorenz.meire@ugent.be)

Published by Copernicus Publications on behalf of the European Geosciences Union.

BGD
11, 17925–17965, 2014

Abstract

The Greenland Ice Sheet releases large amounts of freshwater, which strongly influences the physical and chemical properties of the adjacent fjord systems and continental shelves. Glacial meltwater input is predicted to increase strongly in the future, but the impact of meltwater on the carbonate dynamics of these productive coastal systems remains largely unquantified. Here we present seasonal observations of the carbonate system in the surface waters of a west Greenland tidewater outlet glacier fjord. Our data reveal a permanent undersaturation of CO_2 in the surface layer of the entire fjord and adjacent shelf. The average annual CO_2 uptake for the fjord is estimated to 65 g C m^{-2} yr^{-1} indicating that the fjord system is a strong sink for CO_2. Primary production and the high input of glacial meltwater strongly affect the carbonate system in the Godthåbsfjord system. The largest CO_2 uptake occurs near to the ice sheet. High glacial meltwater input during the summer months correlates strongly with high levels of CO_2 undersaturation, which can be explained by the non-linear effect of salinity on surface water pCO_2 resulting from the mixing of glacial meltwater and ambient fjord water. Our findings hence imply that glacial meltwater may form a major driver for CO_2 undersaturation in fjord and coastal waters adjacent to an Ice Sheet.

1 Introduction

The Arctic Ocean plays an important role in the global carbon cycle and contributes 5–14 % to the global CO_2 uptake (Bates and Mathis, 2009). Intensive biological activity combined with high seasonality in freshwater input and sea ice cover lead to strong dynamics in the carbonate system (Kaltin and Anderson, 2005). Increasing water temperatures, freshwater input and decreasing ice cover will likely have a profound effect on the Arctic Ocean and will likely amplify the large seasonal and spatial biogeochemical gradients that occur in this area (Bates and Mathis, 2009; Mathis et al., 2011). Yet at present, we have still a limited understanding of the carbon dynamics in these high-

BGD
11, 17925–17965, 2014

latitude coastal systems due to the scarcity of studies compared to low latitude coastal environments (Bates and Mathis, 2009). As a result many questions remain on how the carbon cycle in the Arctic will be affected by future environmental changes.

Many of these coastal systems in the Arctic are affected by glacial meltwater input, which leaves a unique biogeochemical fingerprint upon the surface waters. Up to now only a few studies have investigated the CO_2 uptake in Arctic fjord systems impacted by glacial meltwater input (Evans et al., 2013; Rysgaard et al., 2012; Sejr et al., 2011). All these studies report substantial CO_2 undersaturation in the surface water. Data from a seasonal study in the mouth of Godthåbsfjord (SW Greenland) revealed low pCO_2 conditions in the surface water thus leading to high CO_2 uptake rates ($7.2\,t\,C\,month^{-1}\,km^{-2}$). But the exact mechanisms for this strong carbon sink are presently not well understood (Rysgaard et al., 2012). On the one hand, high primary production estimates (of 67 to $500\,g\,C\,m^{-2}\,yr^{-1}$) in West Greenland waters (Jensen et al., 1999; Juul-Pedersen et al., 2014; Rysgaard et al., 2012) indicate that biological processes may have a strong effect on the carbonate dynamics and CO_2 uptake. On the other hand the hypothesis has been put forward by Rysgaard et al. (2012) that glacial meltwater may exert a strong impact on the CO_2 dynamics of Arctic fjord systems. However, the relative importance of biology vs. glacial meltwater input is presently uncertain nor are the mechanisms clear of how glacial meltwater input can stimulate CO_2 uptake.

Accelerated mass loss from the Greenland Ice Sheet and fast climate changes (Rignot et al., 2011) demand a conceptual understanding of how different drivers affect the carbon cycle in high latitude coastal areas. The main focus of this study is to investigate the mechanisms controlling the CO_2 uptake in fjord systems and shelf areas affected by glacial meltwater (Godthåbsfjord, Greenland). To this end, an extensive sampling program was set up involving monthly sampling at three dedicated stations in the fjord, in addition to seasonal transects across the whole fjord and shelf system. Data covering the full annual cycle of partial pressure of CO_2, dissolved inorganic carbon were collected alongside hydrographic and biological measurements. This approach allows

BGD
11, 17925–17965, 2014

us to resolve the seasonal importance of the different drivers in CO_2 uptake and the impact of glacial meltwater on the carbon cycle in these coastal systems.

2 Material and methods

2.1 Field site

This study was conducted in the Godthåbsfjord system (Nuup Kangerlua, southwest Greenland), which covers a total area of 2013 km^2 and has a volume of 525 km^3 (Fig. 1). The mean depth of the fjord is 260 m and there is a sill of 170 m depth located at the entrance of the fjord (Mortensen et al., 2011; Rysgaard et al., 2012). Six outlet glaciers drain into the fjord system. Recent hydrological simulations estimate the annual freshwater input to Godthåbsfjord (excluding solid ice discharge, basal and submarine melt from glaciers) to be 22.5 ± 5.2 km^3 yr^{-1} for the period 1991–2012 (Langen et al., 2014). Ice sheet runoff accounts for 60 % of the freshwater input, land runoff is responsible for 34 %, and net precipitation over the fjord surface represents the remaining 6 % (Langen et al., 2014). Van As et al. (2014) project a similar estimate of 10–20 km^3 glacial ice loss per year for the Godthåbsfjord glaciers.

2.2 Data

Data was collected during four cruises in 2013 (February, May, August and September/October) along a length-transect of 20 stations which covers the fjord and the Fyllas Banke, a part of the West Greenland continental shelf (Fig. 1). The dataset was further complemented by monthly sampling at three selected stations GF3, GF7 and GF10 over the period from May 2012 to December 2013. These 3 sampling stations are representative for 3 different zones in the fjord (Fig. 1). Zone 1 (with GF3 as representative station) comprises the outer part of the fjord (referred to as outer sill region by Mortensen et al., 2011), which is characterized by strong tidal currents. Zone 2 (represented by GF7) covers the central part of the fjord. Finally zone 3 (with GF10 as

BGD
11, 17925–17965, 2014

representative) is the inner part close to the freshwater sources, which is most strongly affected by glacial meltwater.

At each station and sampling time, conductivity and temperature depth profiles were recorded by a CTD instrument (Seabird SBE19+), which was equipped with a fluorescence (Seapoint Chlorophyll Fluorometer) and Photosynthetic Active Radiation sensor (LI-COR 190SA quantum Q PAR sensor). Partial pressure of carbon dioxide (pCO_2) was measured in situ using the HydroC™ Carbon Dioxide Sensor (Contros, Germany) at seven water depths (1, 5, 10, 20, 30, 40 and 50 m). At every depth the HydroC sensor was equilibrated for 2–5 min until a stable reading was obtained.

Water samples were collected at eight water depths (1, 5, 10, 20, 30, 40, 100 and 400 m) using 5 liter Niskin bottles (KC Denmark Research Equipment). Unfiltered water was transferred by gastight tubing (Tygon) to 12.5 mL exetainers (Labco, UK) for dissolved inorganic carbon (DIC) and total alkalinity (TA) analysis. Exetainers were left to overflow and samples were preserved by adding 0.02 % of a saturated $HgCl_2$ solution (Dickson and Goyet, 1992). Samples were stored in darkness at 4 °C until further analysis. DIC was measured using an infra-red DIC analyzer (Apollo SciTech), which consists of an acidification and purging unit in combination with a LI-COR-7000 CO_2/H_2O Gas analyser. Relative SDs for DIC were ±0.1 % ($n = 10$). TA was determined using the standard operating procedure for open cell potentiometric titration (Dickson et al., 2007, SOP 3b), using an automatic titrator (Metrohm 888 Titrando), a high accuracy burrette (1 ± 0.001 mL), a thermostated reaction vessel ($T = 25$ °C) and combination pH glass electrode (Metrohm 6.0259.100). TA values were calculated by a non-linear least-squares fit to the titration data (Dickson et al., 2007, SOP 3b) in a custom-made script in the open source programming framework R (R Core Team, 2013). The relative SD of the procedure was ±0.2 % ($n = 10$). Quality assurance of TA and DIC analysis involved regular analysis of Certified Reference Materials (CRM Batch 126 provided by A. G. Dickson, Scripps Institution of Oceanography).

Water samples for chlorophyll analysis were filtered onto 25 mm GF/F filters (Whatman, nominal pore size of 0.7 µm). Filters were placed in 10 mL of 96 % ethanol for 18

BGD
11, 17925–17965, 2014

to 24 h and chlorophyll fluorescence in the filtrate was analyzed using a fluorometer (TD-700, Turner Designs) before and after addition of 200 µL of a 1 M HCl solution.

Primary production was measured using the ^{14}C incubation method (Nielsen, 1952). Incubation bottles were filled with 55 mL unfiltered seawater and spiked with 175 µL $NaH^{14}CO_3$ (20 µCi mL^{-1}) and incubated for two hours in an ICES incubator (Hydro-Bios, Germany). The samples were filtered onto 25 mm GF/F filters (Whatman) and 100 µL of 1 M HCl was added to remove excess $NaH^{14}CO_3$ and the filters were left open for 24 h in the fume hood. Subsequently, 10 mL of scintillation cocktail (Ultima Gold, Perkin Elmer) was added to the samples before counting them on the scintillation counter (Liquid Scintillation Analyzer, Tri-Carb 2800TR, PerkinElmer). After subtracting fixation rates obtained from the dark incubations, gross primary production rates were calculated based on measured DIC concentrations. Photosynthesis-Irradiance (P-I) curves were obtained for 11 sampling dates at 2 separate depths (5 and 20 m). The light extinction coefficient was calculated from the measured PAR profile. Solar irradiance values were obtained from the meteorological survey in Nuuk (Meteorological station 522, Asiaq Greenland Survey). Using the solar irradiance at each day, the light extinction coefficient and the P-I curves at the monthly sampling dates, the daily productivity was calculated over the entire year. This approach assumes that light extinction and P-I curves remain the same in the two-week period before and after the sampling dates.

Bacterial production was measured using the ^{3}H-thymidine method (Fuhrman and Azam, 1982). Triplicate samples (10 mL) were incubated at in situ temperature. After an incubation of 6 to 8 h, bacterial activity incubations were stopped by adding 500 µL of 100 % trichloroacetic acid (TCA). The samples were subsequently filtered through 25 mm cellulose ester filters (pore size 0.2 µm, Advantec MSF). Equations from Søgaard et al. (2010) were used to calculate bacterial production. For the calculation of the bacterial carbon demand from the bacterial production, a bacterial growth efficiency of 0.5 was used according to Rivkin et al. (2001).

BGD
11, 17925–17965, 2014

The difference in pCO_2 between surface water and atmosphere drives the air–sea CO_2 exchange (ASE). Air–sea CO_2 fluxes were calculated using the relation:

$$\mathrm{ASE} = K_{\mathrm{av}} \alpha \Delta pCO_2 \quad (1)$$

where ΔpCO_2 is the difference in pCO_2 of the surface water (here at 1 m water depth) and the atmospheric pCO_2. Negative values of ASE imply an uptake by the sea and positive values an efflux to the atmosphere. The atmospheric pCO_2 was measured monthly at GF3 using an infrared CO_2 monitor (EGM-4 PP systems). The mean atmospheric pCO_2 was 400 µatm for 2013. The quantity α is the solubility of CO_2 in seawater (mol m^{-3} atm^{-1}). K_{av} (m s^{-1}) is the gas transfer coefficient calculated using both the formulation of Nightingale et al. (2000) and of Wanninkhof and McGillis (1999). These formulations depend on the wind speed data (m s^{-1}), at 10 m a.s.l., obtained from the Nuuk weather station in the fjord system (Meteorological station 522, Asiaq Greenland Survey). The monthly mean wind speed varied from 5 to 9 m s^{-1} for 2012 and 2013 but during storms wind speed peaks up to 30 m s^{-1} were recorded.

Processing of data was done in the open-source programming language R (R Core Team, 2013). The AquaEnv R-package (Hofmann et al., 2010) was used for acid-base speciation and CO_2 system calculations. Interpolation of the data and contour plots were produced using the Akima package (Akima et al., 2006).

2.3 Biogeochemical model

To analyze the impact of the glacial meltwater input on the seasonal carbon dynamics of the fjord system, a simplified biogeochemical model was constructed. The model describes how the pCO_2 dynamics is influenced by the circulation in the fjord (including the input of glacial meltwater), air–sea exchange of CO_2 and net ecosystem production. This biogeochemical model is constrained by data from monthly measurements of 2013 and the seasonal length section data from the fjord system, using an inverse modelling procedure.

BGD
11, 17925–17965, 2014

The biogeochemical model fjord system is composed out of three separate, connected boxes, representing the outer, central and inner part of the fjord system and one large "open sea" box, representing the outer shelf; the latter was added to obtain full mass balance closure. Each box represents the upper 40 m of the water column since this depth range is most strongly affected by primary production (due to light availability) and the glacial meltwater imprint. The model includes a water mass balance in addition to the mass balances of three state variables (salinity, DIC and TA) for each box (Table 1). Once DIC and TA are known, all relevant parameters of the carbonate system (including pCO_2) can be calculated.

2.3.1 Water mass balance

Figure 2 shows a simplified circulation model for the fjord system. Intrusion of coastal water into the fjord, leads to an input of saline water (F_i) in each of the three zones. The inner zone of the fjord experiences an input of glacial meltwater (Q_g). The combination of saline seawater intrusion and freshwater from the glacier results in a return flow (Q_i) in the surface water which is eventually discharged onto the Greenland shelf. The resulting water mass balance equations are shown in Table 1 (Eqs. 1–3, Table 1),. Based on the water mass balance equations, a mass balance can be constructed for salinity in the different zones (Table 1).

The magnitude of the different flows in the fjord system is unknown and these flows are expected to vary strongly throughout the year due to the strong seasonality in the glacial meltwater input as well as seasonal inflows of coastal water (Mortensen et al., 2011). The water mass balance provides 3 independent equations, which allows to constrain the three return flows, $Q_i(t)$, when the seawater inputs, $F_i(t)$, and glacial meltwater input, $Q_g(t)$, are known.

The variation of the glacial meltwater input with time, $Q_g(t)$, was estimated from salinity observations at station GF10 close to the outlet glaciers. The total annual meltwater input into Godthåbsfjord was constrained to be 20 $km^3\,yr^{-1}$ as derived from regional climate model simulations for Godthåbsfjord (Langen et al., 2014; Van As et al., 2014).

BGD
11, 17925–17965, 2014

The relative contribution of freshwater (x) at station GF10 was estimated from a two end-member mixing model ($S = x \cdot S_{FW} + (1 - x) \cdot S_{SW}$) (Sect. 2.3.3.). The contribution x was calculated at each month and fitted with a smoothing spline. Assuming that x scales with $Q_g(t)$, the temporal variation of x was used to predict the temporal variation of Q_g (and ensuring that integrated annual meltwater was equal to 20 $km^3\,yr^{-1}$).

The values of the three remaining seawater inputs ($F_i(t)$) in the different zones were obtained by an inverse modelling approach using the monthly salinity data obtained at the three representative stations (GF3, GF7 and GF10). To this end, we estimated the salinity changes dS_i/dt in the different zones by fitting a cubic smoothing spline (Hastie and Tibshirani, 1990) through the monthly salinity data and subsequently taking the derivative. If we implement both the observed salinities and the salinity changes, we obtain a linear set of three equations (Eqs. 4–6, Table 1), which allows to estimate the seawater inputs ($F_i(t)$).

2.3.2 Dissolved inorganic carbon balance

The different flows as derived from the water mass balance were used to parameterize the transport terms in the mass balances for TA (Eqs. 7–9, Table 1) and DIC (Eqs. 10–12, Table 1). Alkalinity was assumed to behave conservatively within the fjord, and hence was only influenced by transport (Thomas and Schneider, 1999). In contrast, the DIC mass balance accounted for transport processes, but also air–sea exchange of CO_2 (ASE) and net community production (NCP) (Table 1). Air–sea CO_2 fluxes were calculated according to Eq. (1) using the formulation by Nightingale et al. (2000) for the gas transfer coefficient. The pCO_2 concentration of the surface water was calculated from salinity, temperature, TA and DIC using the R package AquaEnv (Hofmann et al., 2010). The net community production (NCP) was calculated as the difference between the primary production (PP) and bacterial carbon demand (BCD) and values for the rate of these processes were determined based on monthly rate measurements. Accordingly, NCP was imposed as a forcing function upon the model.

BGD
11, 17925–17965, 2014

2.3.3 End members composition

The model uses two end-member types of water as input, freshwater from glacial meltwater and saline water. The composition (S, DIC, TA) of both end-member types of water was determined based on collected data. The largest fraction of the freshwater input is from glacial origin and so we used the properties for glacial meltwater for the freshwater end-member. The values were estimated from twenty icebergs samples collected in the fjord. Salinity, DIC and TA were measured after thawing the ice in the laboratory in gas-tights bags ($S_{FW} = 0$, $DIC_{FW} = 80 \pm 17\,\mu mol\,kg^{-1}$, $TA_{FW} = 50 \pm 20\,\mu mol\,kg^{-1}$). For the seawater end-member, we used the properties of deep fjord water (water at 400 m depth) which is shown to be comparable to the properties of the water on the shelf ($S_{SW} = 33.65$, $DIC_{SW} = 2150\,\mu mol\,kg^{-1}$, $TA_{SW} = 2220\,\mu mol\,kg^{-1}$ and $T_{SW} = 2\,^{\circ}C$).

2.3.4 Numerical solution

A numerical solution procedure for the resulting differential equations was implemented in the open-source programming language R following Soetaert and Meysman (2012). The set of differential equations was integrated using the R-package deSolve (Soetaert et al., 2010). The calculation of the carbonate system (and hence pCO_2) at each time step of the numerical simulation was performed via the operator splitting approach as detailed in Hofmann et al. (2008). The resulting pCO_2 concentration then can be employed in the kinetic rate expression for the air–sea CO_2 exchange. The model was run over a full seasonal cycle (representing the year 2013) and with a spin-up period of 2 years. The goodness of fit (GOF) between model simulation output and observational data was calculated as the sum of squared residuals.

BGD
11, 17925–17965, 2014

3 Results

3.1 Spatial variability in the fjord system

The hydrography of Godthåbsfjord is strongly affected by the seasonal input of glacial meltwater. Figure 3 shows the spatial distribution of salinity in the upper 40 m of the water column during four cruises in 2013 (February, May, August and October). The length transects range from the west Greenland continental slope to the inner part of the fjord where six glaciers discharge. Low freshwater runoff during winter and spring months coincides with high salinities ∼ 33 in the upper 40 m of the water column throughout the fjord (Fig. 3a and b). Increased input of glacial meltwater during summer creates a strongly stratified system, where the surface water shows a distinct layer in the central and inner part of the fjord (Fig. 3c). Due to distribution of freshwater sources, the impact is most pronounced at the inner fjord stations (GF9 to GF13) where in August salinity drops to ∼ 8 in a shallow surface water layer of 10 m depth. In the central fjord (GF5 to GF8), summer salinity decreases to 17 and upper layer of low-saline upper water layer extends deeper to 15–20 m depth. In the outer part of the fjord (the outer sill region, GF1 to GF4) the salinity decrease with depth is less pronounced as the freshwater is mixed deeper into the water column by strong tidal mixing. Still, even at the shelf stations (FB1 to FB4), a weak imprint of glacial meltwater can be observed. Decreased input of glacial meltwater during the autumn months coincides with a gradual increase in salinity in the surface layer and a less steep halocline (Fig. 3d).

Strong seasonality was also observed in the fluorescence data (Fig. 4). Evidence of a spring bloom is indicated by high chlorophyll *a* concentrations on the shelf (FB4 to FB1) and in the central fjord (GF5 to GF8) observed during the May cruise (Fig. 4b). In contrast to the May situation, where the chlorophyll *a* is evenly distributed in the upper 40 m of the water column, distinct chlorophyll maxima were observed in August (Fig. 4c). During the August cruise, high fluorescence values of $\sim 6\,\mu g\,L^{-1}$ were observed at the outer shelf stations at approximately 30 m depth (FB4 and FB3.5). Clear chlorophyll *a* maxima also occurred in the central and inner part fjord with values of

BGD
11, 17925–17965, 2014

$\sim 10\,\mu g\,L^{-1}$ at 20 m depth at GF8 and values of $\sim 15\,\mu g\,L^{-1}$ at 10 m depth in the inner fjord (GF9 to GF12). In February and October low chlorophyll *a* concentrations were measured throughout the entire fjord and shelf system (all values lower than $1\,\mu g\,L^{-1}$; note that values are missing for the shelf region in February).

Strikingly, a permanent undersaturation of pCO_2 was observed in the surface waters of the entire fjord system throughout the year (note that only surface pCO_2 data is available for February). Maximum pCO_2 surface values of $\sim 350\,\mu atm$ were measured in February, and at this time, surface pCO_2 did not vary throughout the fjord (Fig. 5a). In May pCO_2 undersaturation became more pronounced, and the lowest values were observed over the shelf and in the surface layer at the inner fjord stations (Fig. 5a). At the shelf stations, low pCO_2 values ($< 240\,\mu atm$) were observed throughout the water column and these coincided with DIC concentrations lower than $2000\,\mu mol\,kg^{-1}$ that were also homogeneous throughout the water column (Figs. 5b and 6a). Despite the occurrence of low pCO_2 values ($\sim 200\,\mu atm$) coinciding with low DIC ($\sim 1950\,\mu mol\,kg^{-1}$) in the surface layer of the inner fjord stations, high pCO_2 values ($> 300\,\mu atm$) and high DIC concentrations ($> 2000\,\mu mol\,kg^{-1}$) were observed in the layer below 20 m depth (Figs. 5b and 6a).

In August a further decrease in surface pCO_2 was observed in the central and inner part of the fjord (Fig. 5c). Undersaturation was strongest at stations closest to the tidewater outlet glaciers where pCO_2 values as low as 74 µatm were measured (Fig. 5c). At this time, the DIC concentration also dropped below $800\,\mu mol\,kg^{-1}$ in the upper meters of the water column (Fig. 6b). Below this shallow layer of low-saline water, DIC concentrations and pCO_2 values increased strongly with depth, reaching respectively $\sim 2000\,\mu mol\,kg^{-1}$ and $\sim 330\,\mu atm$ at 40 m depth. The water layer depleted in pCO_2 and DIC extends to greater depth in the central region of the fjord (GF5-GF8, Figs. 5c and 6d) but the undersaturation in the surface is not as pronounced compared to the stations close to the tidewater glaciers. For the stations on the shelf, the pCO_2 values in August were similar to those observed in May (Fig. 5a) though a subsurface minimum

BGD
11, 17925–17965, 2014

with pCO_2 values lower than 220 µatm was observed at 30 m depth at one of the slope stations (FB3.5, Fig. 5c).

In October pCO_2 and DIC values in the surface waters gradually increased again compared to the previous campaigns (Figs. 5a and 6c). The lowest values were still found in the inner part of the fjord (Figs. 5d and 6c). Gradients with depth were not as strong, most likely due to reduced stratification (Fig. 3d).

Good linear relationships between DIC vs. salinity (R squared 0.92; DIC = 61 + 59S) and TA vs. salinity (R squared 0.95; TA = 159 + 63S) are observed indicating that they follow conservative mixing.

3.2 Annual variability close to glaciers

Time series from the station GF10, located in the inner fjord system (Fig. 1), show the seasonal evolution in the depth-averaged values (0–40 m) for salinity and temperature (Fig. 7a), the parameters of the carbonate system (Fig. 7b), chlorophyll *a* (Fig. 7c) and primary production and bacterial carbon demand (Fig. 7d). The mean salinity in the upper water column was ~ 33 during late winter and spring when freshwater runoff to the fjord is at its minimum (Fig. 7a). Around early June salinity started to decrease rapidly and attained its annual minimum (~ 27 in 2013) in August, corresponding to the period of highest freshwater input due to glacial melt. From August onwards to late winter, salinity showed a gradual increase after which values remained constant from March to June. Temperature ranged from 0.5 to 3.5 °C and showed a more irregular seasonal pattern. Lowest temperature was observed in February whereas the highest in October. During the period from March to August 2013, the depth-averaged temperature fluctuated around 1.5 °C (Fig. 7a).

The seasonal cycle of the carbonate system tracked the temporal evolution of salinity. Values of pCO_2, DIC and TA showed a gradual increase during the winter months in the upper 40 m. Maximum values were obtained in March with depth-averaged values of pCO_2 ~ 350 µatm, DIC ~ 2040 µmol kg^{-1} and TA ~ 2200 µmol kg^{-1}. In April 2013, the pCO_2 dropped rapidly and reached ~ 250 µatm by the mid of May, while the average

BGD
11, 17925–17965, 2014

DIC concentration in the upper 40 m simultaneously decreased to ~ 1950 µmol kg^{-1} (Fig. 7b). Coinciding with this spring decrease in DIC and pCO_2, high chlorophyll *a* concentrations were observed (Fig. 7c). High primary production rates match the high chlorophyll *a* concentrations and also bacterial carbon demand increased (Fig. 7d). During the subsequent summer months, DIC in the upper 40 m decreased to an average concentration of 1850 µmol kg^{-1} in 2013 (and ~1700 µmol kg^{-1} in 2012), coinciding with the strong salinity decrease due to glacial meltwater runoff. The alkalinity shows a similar decrease in response to the increase in freshwater input. Despite the strong pCO_2 decrease in the upper 20 m, with concentrations down to 100 µatm in the surface water of the inner fjord (Fig. 5c), the summer decrease of pCO_2 at GF10 as shown in Fig. 7b was less pronounced (minimum at ~ 200 µatm) due to depth averaging (mean over 0–40 m layer). Continued primary production and bacterial carbon demand was observed after the spring bloom although rates are lower and depth averaged chlorophyll *a* values lay around 2–3 µg L^{-1} (Fig. 7c and d). From October onwards, the pCO_2, TA and DIC concentration started to increase slowly to reach the maximal winter values, while chlorophyll *a* values were negligible.

Measurements of primary production and bacterial carbon demand allow to estimate net community production in station GF10, giving a value of 85 g C m^{-2} yr^{-1} for 2013.

3.3 Air–sea exchange of CO_2 in the fjord system

Using the monthly surface pCO_2 data collected at three stations (GF3, GF7 and GF10) over 2013, the air–sea CO_2 flux can be quantified using wind speed data from the meteorological station at Nuuk (Fig. 8a). Permanent pCO_2 undersaturation leads to a CO_2 uptake during the entire year (Fig. 8b). Depending on the formulation of the gas transfer coefficient (Nightingale et al., 2000; Wanninkhof and McGillis, 1999), the mean annual CO_2 uptake at the inner fjord station GF10 is 70 to 82 g C m^{-2} yr^{-1}. The GF7 station in the central fjord showed an average uptake of 60 to 66 g C m^{-2} yr^{-1}, while the uptake was 37 to 39 g C m^{-2} yr^{-1} at GF3 in the outer part. Based on data from

BGD
11, 17925–17965, 2014

these three stations, an area-averaged annual CO_2 uptake in the entire fjord system is estimated to be $\sim 65\,g\,C\,m^{-2}\,yr^{-1}$.

The mean CO_2 uptake was also calculated for the seasonal transects in May, August and October based on the measured pCO_2 surface data and using the daily wind speed values during the month that spans the sampling date. Confirming the pattern observed at the three monitoring stations, the uptake is higher close to the glaciers and lower in stations downstream the fjord, but rises slightly again over the shelf (Fig. 8c). Lower surface pCO_2 in the central and inner fjord led to almost a doubling of the CO_2 uptake in the inner part of the fjord compared to the outer part. Anova analysis indicates that uptake is significantly different between stations and between different months ($P < 0.001$).

3.4 Model results: driving factors of the carbon dynamics

To resolve the importance of the different driving forces of CO_2 uptake in the fjord, a simplified biogeochemical model was used to simulate the DIC and pCO_2 in the region closest to the glacier (GF10, zone 3) (Fig. 2). This zone is most strongly affected by glacial meltwater input and primary production, and hence, shows the highest excursions in the parameters of the carbonate system. Figure 9 shows the simulated annual cycle of DIC and pCO_2 at GF10 compared with the measured data. Simulations were performed (1) with and without the effect of net community production on carbon dynamics and (2) with a constant temperature throughout the year (the average mean winter temperature in upper 40 m 0.5 °C) or with a variable temperature based on the observations. Simulations that include NCP manage to reproduce the DIC and pCO_2 evolution better as quantified by goodness of fit. NCP has especially a strong effect on the evolution of the pCO_2. The inclusion of seasonal temperature variation had overall a moderate effect on the simulation output. Higher temperatures during summer and autumn (1.5 to 3 °C, Fig. 7a) led to a reduction of pCO_2 undersaturation in the simulation with variable temperature.

BGD
11, 17925–17965, 2014

Figure 10 summarizes how transport processes (including the input of glacial meltwater), air–sea exchange and biological processes affect the change in DIC concentration in GF10. The DIC dynamics shows 3 distinct periods. From January to March, the net change in DIC is positive and DIC increases slowly to maximum values (Period I). DIC subsequently decreases strongly in April coinciding with high NCP (Period II). In July and August, a second decrease in DIC is observed (Period III) coinciding with strong input of glacial meltwater. From September onwards the DIC concentration starts to increase again to its maximum winter values (Period I).

4 Discussion

4.1 Air–sea CO_2 exchange in fjord and coastal waters adjacent to the Greenland Ice Sheet

The surface waters of the shelf area (Fyllas Banke) and the Godthåbsfjord fjord system were strongly undersaturated in CO_2 relative to the atmosphere during the entire year (Fig. 5), and this strong undersaturation leads to a high uptake of CO_2. Based on our data from monthly measurements during 2012–2013 at 3 stations in the fjord, we calculated a mean annual CO_2 uptake of $65\,g\,C\,m^{-2}\,yr^{-1}$. This estimate is lower than the uptake of 83 to $108\,g\,C\,m^{-2}\,yr^{-1}$ estimated earlier for the outer sill region of Godthåbsfjord (Rysgaard et al., 2012). The difference between both estimates can possibly be explained by strong interannual variability in the flux (Rysgaard et al., 2012). Our estimate for the CO_2 uptake in Godthåbsfjord is higher than values previously reported from other sites in Greenland, such as $52\,g\,C\,m^{-2}\,yr^{-1}$ in the Greenland sea; (Nakaoka et al., 2006) and $32\,g\,C\,m^{-2}\,yr^{-1}$ in Young Sound, a fjord in Northeast Greenland (Sejr et al., 2011), indicating that Godthåbsfjord is a strong sink of CO_2. Our estimates for the CO_2 uptake at the Fyllas Banke shelf area (0.15 to $0.6\,g\,C\,m^{-2}\,d^{-1}$) are also substantially higher than the average uptake of $0.04\,g\,C\,m^{-2}\,d^{-1}$ reported by Chen et al. (2013)

BGD
11, 17925–17965, 2014

for other shelf systems areas located higher than 50° N. This indicates that the coast off Southwest Greenland is also an important sink for CO_2.

4.2 Effect of glacial melt on the carbon dynamics

Our data shows the strongest pCO_2 undersaturation (Fig. 5a and c) and highest CO_2 uptake in the inner part of the Godthåbsfjord system (Fig. 8). High CO_2 uptake has been reported before in fjord systems affected by glacial meltwater (Rysgaard et al., 2012; Sejr et al., 2011; Torres et al., 2011) indicating that glacial melt could affect the carbon dynamics and drive CO_2 uptake. However, until now, the actual mechanism of how that glacial melt could induce strong pCO_2 undersaturation has not been elucidated.

Glacial meltwater can affect pCO_2 undersaturation in different ways. First of all, the meltwater itself is slightly undersaturated in pCO_2. We collected iceberg samples in the Godthåbsfjord area, which showed concentrations of DIC of $80 \pm 17\,\mu mol\,kg^{-1}$ and TA of $54 \pm 20\,\mu mol\,kg^{-1}$, yielding a pCO_2 value of $\sim 350\,\mu atm$. Accordingly, the meltwater is slightly undersaturated compared to the measured atmospheric CO_2 values of $\sim 400\,\mu atm$. Input of glacial ice and subsequent melting will consequently create a CO_2 sink in Godthåbsfjord. Using a pCO_2 undersaturation of $\sim 350\,\mu atm$ and a glacial freshwater discharge of $20\,km^{-3}\,yr^{-1}$ to the fjord system (Langen et al., 2014; Van As et al., 2014), this could directly account for an uptake of $0.5–2.0\,g\,C\,m^{-2}\,yr^{-1}$ in Godthåbsfjord. This direct effect of glacial meltwater on pCO_2 undersaturation hence only accounts for a minor fraction of CO_2 uptake in the fjord system (1–3 % of the annual CO_2 uptake estimated to be $65\,g\,C\,m^{-2}\,yr^{-1}$).

A second mechanism via which glacial meltwater can induce pCO_2 undersaturation is the non-conservative behavior of pCO_2 during the mixing of fresh water and saline water. As it happens, this mixing effect could explain a large part of the low pCO_2 (and consequent CO_2 sink) that we observed in the Greenland fjord systems. The mechanism can be understood by considering the mixing of two water parcels with

BGD
11, 17925–17965, 2014

different composition. When mixing is conservative, the concentration of a chemical compound obeys the relation

$$[E]_{\mathrm{Mix}}(M_1 + M_2) = [E]_1 M_1 + [E]_2 M_2 \quad (2)$$

where $[E]$ is the concentration of the compound E and M are the masses of the water parcels. Salinity, TA and DIC are conservative quantities with respect to mixing (Wolf-Gladrow et al., 2007). However, the fact that TA and DIC mix conservatively, does not imply that pCO_2 will behave conservatively upon mixing. In other words, if two water parcels, initially in equilibrium with the atmosphere, mix, it does not imply that the resulting mixture will also be in equilibrium with the atmosphere. In fact, mixing of fresh water and saline water induces a strong pCO_2 undersaturation. Figure 11a shows the undersaturation created when two water masses at equilibrium are mixed, one with low salinity, low TA and low DIC (representative for a water parcel from glacial origin) and one with high salinity, high TA and high DIC (representative for saline fjord water). The mixture of these two parcels will be undersaturated in pCO_2 due to the non-linear effect of salinity on pCO_2. Consequently this water parcel will take up CO_2 when in contact with the atmosphere (Fig. 11a). Note that the strongest undersaturation is obtained when the resulting mixture has a salinity of ~ 8 and that pCO_2 undersaturation can exceed 200 µatm below the atmospheric level (Fig. 11a). This salinity effect on pH and pCO_2 dynamics has been described previously for estuarine systems (Mook and Koene, 1975; Whitfield and Turner, 1986) but as yet, the mechanism has not been invoked for glacier affected systems. In fjord systems affected by glacial melt, meltwater (with low TA, DIC and salinity) mixes with ambient fjord waters (with high TA, DIC and salinity). This mechanism hence could constitute an important driver for pCO_2 undersaturation when sufficiently large amounts of meltwater are discharged into the fjord, so that salinity levels are sufficiently reduced. The undersaturation that has been previously observed in other systems affected by glacier melt water (Evans et al., 2014; Sejr et al., 2011; Torres et al., 2011) might possibly be explained by this same mechanism.

BGD
11, 17925–17965, 2014

In Godthåbsfjord, pCO_2 undersaturation is strongest during the summer months when large volumes of meltwater are mixed with fjord water and salinity in surface layer drops to ∼ 8 (which coincides with the maximum undersaturation observed in Fig. 11a). The correlation in the timing of pCO_2 undersaturation and meltwater discharge suggests that the salinity effect described above could be the main driver of the observed pCO_2 undersaturation. To verify this hypothesis, we used the salinity depth profiles recorded in August 2013 at the three monitoring stations. We calculated the associated pCO_2 depth profile, assuming that only the salinity effect is playing and that no other processes (such as air–sea exchange and NCP) are affecting the pCO_2 depth profile (Fig. 11b).

Close to the glacier in the upper meters where high volumes of both water masses are mixed (Zone 2 and 3), a strong undersaturation effect is observed where pCO_2 values drop below 200 µatm (Fig. 11b). This indicates that glacier melt water input is indeed an important driver for the strong pCO_2 undersaturation and high CO_2 uptake as observed in summer in the inner part of Godthåbsfjord. Based on our simulations with the hydrological model for the fjord system (Table 1), we estimated that this mechanism could be responsible for an uptake of 10–20 $g\,C\,m^{-2}\,yr^{-1}$ in the Godthåbsfjord system which constitutes 15–30 % of the total CO_2 uptake by the fjord system. Note that this should be regarded as a minimal estimate. The biogeochemical model assumes homogenized conditions over the 40 m water depth, and may thus underestimate the pCO_2 undersaturation in the upper water layer (Fig. 11b).

4.3 A seasonal cycle in a glacial meltwater affected fjord

In addition to the input of glacial meltwater, other driving forces are affecting the annual cycle of the carbonate system in Godthåbsfjord. The importance of different factors differs in strength across the seasonal cycle. Our data suggest three distinct phases in the annual cycle, which is represented by the scheme in Fig. 10.

BGD
11, 17925–17965, 2014

4.3.1 Phase I: autumn and winter period

During autumn, glacier melting decreases and freshwater runoff to the fjord slowly diminishes (Figs. 3 and 7). Combined with dense coastal inflows to the fjord, this leads to a gradual salinity increase in the upper water layer and flushing of accumulated freshwater out of the Godthåbsfjord system (Fig. 7) (Mortensen et al., 2011, 2013). Weakening of the surface stratification combined with strong winter storms lead to a stronger mixing of the upper water layers. DIC and pCO_2 concentration increases slowly due to advection of water masses with high DIC and pCO_2 (upwelling of fjord deep water) and continued air–sea exchange to reach an average pCO_2 of ~350 µatm (Figs. 7, 8 and 10).

4.3.2 Phase II: spring bloom

At the start of April, a strong spring bloom is observed in the inner part of the fjord, leading to high chlorophyll *a* concentrations, high net primary production and strong CO_2 uptake (Fig. 7). The high biological carbon uptake decreases the DIC and lowers the pCO_2 to 250 µatm in the surface waters of the inner fjord (GF10) by the middle of May (Figs. 7 and 10). The strong effect of primary production on the pCO_2 is observed in the entire fjord system in May (Figs. 4 and 5). Low surface water pCO_2 concentrations occur in almost the entire fjord system and on the shelf. During this period, the impact of the glacial meltwater on the fjord system is not pronounced, and the upper water column is still well mixed (Mortensen et al., 2011, 2013). Consequently low pCO_2 occur at nearly constant salinity and the undersaturation is almost homogenous in the water column. This matches with the evenly distribution of the fluorescence in the upper 40 m (Figs. 3–5). Only in the inner part of the fjord a clear gradient in pCO_2 with water depth can be observed. Continued inflow of dense water into the fjord system leads to upwelling in the inner part of the fjord, bringing up the deep water masses rich in DIC and pCO_2 (Figs. 3 and 5) (Mortensen et al., 2011).

BGD
11, 17925–17965, 2014

The strong effect of biological processes on pCO_2 is illustrated in Fig. 9. In a model simulation without NCP, the large drop in pCO_2 concentrations observed in the spring and summer data is not reproduced. The high pCO_2 undersaturation in the spring is consequently linked to high biological activity (Bates and Mathis, 2009; Shadwick et al., 2011; Thomas and Schneider, 1999). Combined with the high primary production rates, high vertical fluxes of chlorophyll *a* from sediment traps are observed in the fjord at this time, indicating that a large fraction of the organic material produced in the upper water layers sinks to deeper waters (Rysgaard et al., 2012). Primary production is consequently able to counteract the large CO_2 air–sea influxes and to maintain low pCO_2 in surface water (Figs. 5 and 9b). This creates an efficient biological pump through the spatial separation of production and mineralization (Sejr et al., 2014; Thomas et al., 2004).

4.3.3 Phase III: summer glacial melt

After the initial decrease in spring, surface water DIC decreases further during summer, coinciding with the increased input and mixing of glacial melt water into the fjord. At the start of summer (June), glacial meltwater runoff initiates the lowering of the salinity in the upper water layers (Figs. 3 and 7). This freshwater input induces stratification in the upper part of the water column of the inner and central fjord (Fig. 3). The high freshwater input ($\sim 20\,km^3\,yr^{-1}$) has not only a strong effect on fjord hydrography (Mortensen et al., 2011) but also strongly affects the chemistry in the fjord system (Rysgaard et al., 2012) and biology (Arendt et al., 2013). Mixing of glacial meltwater with fjord water strongly reduces the salinity of upper water layers (Figs. 3 and 7) while also DIC and TA are diluted in the upper water layers (Fig. 7). Coincident with this dilution of DIC and TA, a notable strengthening of the pCO_2 undersaturation in the upper water can be observed, as pCO_2 decreased further from 250 to 100 µatm in the upper meter (Fig. 5). This leads to very low pCO_2 in the inner part of the fjord, close to the outlet glaciers and consequently a strong uptake of CO_2 (Fig. 8). Our analysis shows that the non-linear effect of salinity on pCO_2, induced by the mixing of glacial meltwater with fjord

BGD
11, 17925–17965, 2014

water, plays an important role in this observed summer reduction of pCO_2 (Sect. 5.2). In a simulation without biology, a drop in pCO_2 in the upper meters of the surface waters is predicted (Fig. 9b). The water column is however highly stratified and despite the very low values in the upper water layer, higher pCO_2 values are observed at 40 m depth. Subglacial melt plumes, discharging at the grounding line of the glacier (or at other submarine levels), bring up deep water rich in DIC and pCO_2 close to the glacier. This creates a strongly stratified layer with freshwater on top and subglacial meltwater found below 10 m depth as described by Mortensen et al. (2013). The input of subglacial water consequently balances the strong decrease in the upper meters leading to no obvious changes in the mean (0–40 m) pCO_2 during summer period (Fig. 7).

In addition to the large effect of glacial meltwater input, primary production remains a strong driver on DIC and pCO_2 dynamics during summer. Continued high production maintains low pCO_2 on the continental shelf area. Also in the inner fjord continued biological activity (with significant blooms) can be observed (Figs. 4, 5, 7 and 10). The input of glacial meltwater strongly reduces the alkalinity in the upper water layers affecting the buffering of the system (Reisdorph and Mathis, 2014; Torres et al., 2011). Consequently the system becomes extra susceptible to pCO_2 changes. Due to the low buffering capacity, a similar production at lower salinity (and TA values) in the upper water layers has a much stronger effect on pCO_2 and hence even the lower level of primary production during summer can keep pCO_2 at their low levels. Consequently primary production keeps acting as a driving force for creating undersaturation in the fjord system even though mean chlorophyll is lower compared to the spring months (Fig. 7). Measurements of net community production estimate the strength of the biological carbon pump to be 85 g C m^{-2} yr^{-1} indicating that biological processes are the most important driver for carbon dynamics in the fjord responsible for 70–85 % of the total CO_2 uptake by the fjord system. However part of the biological activity can potentially be associated with glacial processes due to the subglacial freshwater discharge. Next to the upwelling of carbon rich water, subglacial freshwater discharge leads to a strong upwelling of nutrients fuelling continuous productivity during the summer in

BGD
11, 17925–17965, 2014

the inner part of the fjord. Consequently both glacial meltwater and primary production can be considered as crucial drivers for the CO_2 uptake in coastal areas affected by glacial meltwater.

Part of the low pCO_2 created by glacial meltwater and biological processes in the fjord is however compensated by higher temperatures in summer and autumn which reduce the CO_2 solubility in water, therefor counteracting the established undersaturation (Fig. 9) (Shadwick et al., 2011; Takahashi et al., 2002). Higher temperatures reduce pCO_2 up to 50 µatm (Fig. 9), reducing the CO_2 uptake with 10–20 % compared to constant temperature simulation.

5 Summary and outlook

Our observations show that Godthåbsfjord is a strong sink for CO_2 due to high biological carbon uptake and undersaturation induced by the input of glacial meltwater. During winter, absence of significant glacial meltwater and biological consumption brings the fjord waters near equilibrium with the atmosphere due to air–sea exchange. A strong bloom during spring leads to a decrease in DIC and pCO_2 indicating the importance of biological processes. During summer, primary production continues to play a central role in the carbon dynamics. But the input and mixing of glacial melt water also plays a crucial role during the summer months. The non-linear effect of salinity on surface water pCO_2 from the mixing of glacial meltwater and saline fjord water creates a strong pCO_2 undersaturation and CO_2 uptake, a mechanism that was yet undescribed for glacial systems.

The processes driving the DIC and pCO_2 dynamics in Godthåbsfjord most likely also apply for other fjord systems and coastal settings that are affected by glacier meltwater. Consequently coastal areas of Greenland and other glacier-influenced areas probably constitute a much larger sink compared to other coastal areas and play a more important role in the high-latitude carbon cycle. Increased melting is anticipated as a result of climate change and will likely accelerate processes affecting carbon dynamics; it will in-

BGD
11, 17925–17965, 2014

crease the freshwater volume mixing in fjord systems and consequently likely enhance the sink for CO_2 in fjord systems affected by glacial melt.

Acknowledgements. This research was supported by the Research Foundation Flanders (FWO aspirant grant to L. Meire) and the Department for Education, Church, Culture and Equality (IIKNN Greenland). D. H. Søgaard was financially supported by the Commission for Scientific Research in Greenland (KVUG). J. Mortensen was financially supported by DEFROST under Nordic Centers of Excellence (NCoE) program. F. J. R. Meysman was financially supported by the Netherlands Organization for Scientific Research (ZKO project on Coastal Acidification), Research Foundation Flanders (FWO-Odysseus grant G.0929.08) and the European Research Council (ERC Starting grant 306933). S. Rysgaard was funded by the Canada Excellence Research Chair program. We thank Asiaq (Greenland Survey) for supplying the irradiance data. This study was conducted in collaboration with the marine monitoring program MarineBasis-Nuuk, part of the Greenland Ecosystem Monitoring (GEM). This work is a contribution to the Arctic Science Partnership (ASP) and the ArcticNet Networks of Centers of Excellence programs. We would like to thank Flemming Heinrich, Maia Olsen, Thomas Krogh and the crew of RV *SANNA* for field and laboratory assistance.

References

Akima, H., Gebhardt, A., Petzoldt, T., and Maechler, M.: Akima: Interpolation of Irregularly Spaced Data, R Packag. version 0.5–1, available at: http://cran.r-project.org/web/packages/akima (last access: 14 December 2014), 2006.

Arendt, K. E., Juul-Pedersen, T., Mortensen, J., Blicher, M. E., and Rysgaard, S.: A 5 year study of seasonal patterns in mesozooplankton community structure in a sub-Arctic fjord reveals dominance of *Microsetella norvegica* (Crustacea, Copepoda), J. Plankton Res., 35, 105–120, doi:10.1093/plankt/fbs087, 2013.

Bates, N. R. and Mathis, J. T.: The Arctic Ocean marine carbon cycle: evaluation of air-sea CO_2 exchanges, ocean acidification impacts and potential feedbacks, Biogeosciences, 6, 2433–2459, doi:10.5194/bg-6-2433-2009, 2009.

Chen, C.-T. A., Huang, T.-H., Chen, Y.-C., Bai, Y., He, X., and Kang, Y.: Air–sea exchanges of CO_2 in the world's coastal seas, Biogeosciences, 10, 6509–6544, doi:10.5194/bg-10-6509-2013, 2013.

BGD
11, 17925–17965, 2014

Dickson, A. and Goyet, C.: Handbook of Methods for the Analysis of the Various Parameters of the Carbon Dioxide System in Sea Water, available at: http://cdiac.esd.ornl.gov/oceans/DOE_94.pdf (Accessed 2 September 2014), 1992.
Dickson, A. G., Sabine, C. L., and Christian, J. R. (Eds.): Guide to best practices for ocean CO_2 measurements, PICES Special Publication 3, 191 pp., 2007.
Evans, W., Mathis, J. T., and Cross, J. N.: Calcium carbonate corrosivity in an Alaskan inland sea, Biogeosciences, 11, 365–379, doi:10.5194/bg-11-365-2014, 2014.
Fuhrman, J. A. and Azam, F.: Thymidine incorporation as a measure of heterotrophic bacterioplankton production in marine surface waters: evaluation and field results, Mar. Biol., 66, 109–120, doi:10.1007/BF00397184, 1982.
Hastie, T. J. and Tibshirani, R.: Generalized Additive Models, Chapman and Hall, London, 1990.
Hofmann, A. F., Meysman, F. J. R., Soetaert, K., and Middelburg, J. J.: A step-by-step procedure for pH model construction in aquatic systems, Biogeosciences, 5, 227–251, doi:10.5194/bg-5-227-2008, 2008.
Hofmann, A. F., Soetaert, K., Middelburg, J. J., and Meysman, F. J. R.: AquaEnv: an aquatic acid-base modelling environment in R, Aquat. Geochem., 16, 507–546, doi:10.1007/s10498-009-9084-1, 2010.
Jensen, H. M., Pedersen, L., Burmeister, A., and Hansen, B. W.: Pelagic primary production during summer along 65 to 72° N off West Greenland, Polar Biol., 21, 269–278, doi:10.1007/s003000050362, 1999.
Juul-Pedersen, T., Arendt, K., Mortensen, J., Blicher, M., Søgaard, D., and Rysgaard, S.: Seasonal and interannual phytoplankton production in a sub-arctic tidewater outlet glacier fjord, west Greenland, Submitt. to MEPS, 2014.
Kaltin, S. and Anderson, L. G.: Uptake of atmospheric carbon dioxide in Arctic shelf seas: evaluation of the relative importance of processes that influence pCO_2 in water transported over the Bering–Chukchi Sea shelf, Mar. Chem., 94, 67–79, doi:10.1016/j.marchem.2004.07.010, 2005.
Langen, P. L., Mottram, R. H., Christensen, J. H., Boberg, F., Rodehacke, C. B., Stendel, M., Van As, D., Ahlstrøm, A. P., Mortensen, J., Rysgaard, S., Petersen, D., Svendsen, K. H., Aðalgeirsdóttir, G., and Cappelen, J.: Recent changes in energy and freshwater budgets for the Godthåbsfjord catchment simulated in a 5 km regional climate model, J. Climate, in review, 2014.

BGD
11, 17925–17965, 2014

Mathis, J. T., Cross, J. N., and Bates, N. R.: Coupling primary production and terrestrial runoff to ocean acidification and carbonate mineral suppression in the eastern Bering Sea, J. Geophys. Res., 116, 2156–2202, doi:10.1029/2010JC006453, 2011.
Mook, W. G. and Koene, B. K. S.: Chemistry of dissolved inorganic carbon in estuarine and coastal brackish waters, Estuar. Coast. Mar. Sci., 3, 325–336, doi:10.1016/0302-3524(75)90032-8, 1975.
Mortensen, J., Lennert, K., Bendtsen, J., and Rysgaard, S.: Heat sources for glacial melt in a sub-Arctic fjord (Godthåbsfjord) in contact with the Greenland Ice Sheet, J. Geophys. Res., 116, 1–13, doi:10.1029/2010JC006528, 2011.
Mortensen, J., Bendtsen, J., Motyka, R. J., Lennert, K., Truffer, M., Fahnestock, M., and Rysgaard, S.: On the seasonal freshwater stratification in the proximity of fast-flowing tidewater outlet glaciers in a sub-Arctic sill fjord, J. Geophys. Res.-Ocean., 118, 1382–1395, doi:10.1002/jgrc.20134, 2013.
Nakaoka, S.-I., Aoki, S., Nakazawa, T., Hashida, G., Morimoto, S., Yamanouchi, T., and Inoue, H. Y.: Temporal and spatial variations of oceanic pCO_2 and air–sea CO_2 flux in the Greenland Sea and the Barents Sea, Tellus B, 58, 148–161, doi:10.1111/j.1600-0889.2006.00178.x, 2006.
Nielsen, E. S.: The use of radio-active carbon (C14) for measuring organic production in the sea, J. Conseil., 18, 117–140, 1952.
Nightingale, P. D., Malin, G., Law, C. S., Watson, A. J., Liss, P. S., Liddicoat, M. I., Boutin, J., and Upstill-Goddard, R. C.: In situ evaluation of air–sea gas exchange parameterizations using novel conservative and volatile tracers, Global Biogeochem. Cy., 14, 373–387, doi:10.1029/1999GB900091, 2000.
R Core Team: R Development Core Team, R A Lang. Environ. Stat. Comput., available at: http://www.R-project.org, 2013.
Reisdorph, S. C. and Mathis, J. T.: The dynamic controls on carbonate mineral saturation states and ocean acidification in a glacially dominated estuary, Estuar. Coast. Shelf S., 144, 8–18, doi:10.1016/j.ecss.2014.03.018, 2014.
Rignot, E., Velicogna, I., Van Den Broeke, M. R., Monaghan, A., and Lenaerts, J.: Acceleration of the contribution of the Greenland and Antarctic ice sheets to sea level rise, Geophys. Res. Lett., 38, L05503, doi:10.1029/2011GL046583, 2011.
Rivkin, R. B. and Legendre, L.: Biogenic carbon cycling in the upper ocean: effects of microbial respiration, Science, 291, 2398–400, doi:10.1126/science.291.5512.2398, 2001.

BGD
11, 17925–17965, 2014

Rysgaard, S., Mortensen, J., Juul-Pedersen, T., Sørensen, L. L., Lennert, K., Søgaard, D. H., Arendt, K. E., Blicher, M. E., Sejr, M. K., and Bendtsen, J.: High air–sea CO_2 uptake rates in nearshore and shelf areas of Southern Greenland: temporal and spatial variability, Mar. Chem., 128–129, 26–33, doi:10.1016/j.marchem.2011.11.002, 2012.

Sejr, M. K., Krause-Jensen, D., Rysgaard, S., Sørensen, L. L., Christensen, P. B., and Glud, R. N.: Air–sea flux of CO_2 in arctic coastal waters influenced by glacial melt water and sea ice, Tellus B, 63, 815–822, doi:10.1111/j.1600-0889.2011.00540.x, 2011.

Sejr, M. K., Krause-Jensen, D., Dalsgaard, T., Ruiz-Halpern, S., Duarte, C. M., Middelboe, M., Glud, R. N., Bendtsen, J., Balsby, T. J. S., and Rysgaard, S.: Seasonal dynamics of autotrophic and heterotrophic plankton metabolism and PCO_2 in a subarctic Greenland fjord, Limnol. Oceanogr., 59, 1764–1778, doi:10.4319/lo.2014.59.5.1764, 2014.

Shadwick, E. H., Thomas, H., Azetsu-Scott, K., Greenan, B. J. W., Head, E., and Horne, E.: Seasonal variability of dissolved inorganic carbon and surface water pCO_2 in the Scotian Shelf region of the Northwestern Atlantic, Mar. Chem., 124, 23–37, doi:10.1016/j.marchem.2010.11.004, 2011.

Soetaert, K. and Meysman, F.: Reactive transport in aquatic ecosystems: rapid model prototyping in the open source software R, Environ. Modell. Softw., 32, 49–60, doi:10.1016/j.envsoft.2011.08.011, 2012.

Soetaert, K., Petzoldt, T., and Setzer, R. W.: Package deSolve: solving initial value differential equations in R, J. Stat. Softw., 33, 1–25, available at: http://www.jstatsoft.org/v33/i09/paper (last access: 14 December 2014), 2010.

Søgaard, D., Kristensen, M., Rysgaard, S., Glud, R., Hansen, P., and Hilligsøe, K.: Autotrophic and heterotrophic activity in Arctic first-year sea ice: seasonal study from Malene Bight, SW Greenland, Mar. Ecol.-Prog. Ser., 419, 31–45, doi:10.3354/meps08845, 2010.

Takahashi, T., Sutherland, S. C., Sweeney, C., Poisson, A., Metzl, N., Tilbrook, B., Bates, N., Wanninkhof, R., Feely, R. A., Sabine, C., Olafsson, J., and Nojiri, Y.: Global sea–air CO_2 flux based on climatological surface ocean pCO_2, and seasonal biological and temperature effects, Deep-Sea Res. Pt. II, 49, 1601–1622, doi:10.1016/S0967-0645(02)00003-6, 2002.

Thomas, H. and Schneider, B.: The seasonal cycle of carbon dioxide in Baltic Sea surface waters, J. Marine Syst., 22, 53–67, doi:10.1016/S0924-7963(99)00030-5, 1999.

Thomas, H., Bozec, Y., Elkalay, K., and de Baar, H. J. W.: Enhanced open ocean storage of CO_2 from shelf sea pumping, Science, 304, 1005–1008, doi:10.1126/science.1103193, 2004.

BGD
11, 17925–17965, 2014

Torres, R., Pantoja, S., Harada, N., González, H. E., Daneri, G., Frangopulos, M., Rutllant, J. A., Duarte, C. M., Rúiz-Halpern, S., Mayol, E., and Fukasawa, M.: Air–sea CO_2 fluxes along the coast of Chile: from CO_2 outgassing in central northern upwelling waters to CO_2 uptake in southern Patagonian fjords, J. Geophys. Res., 116, C09006, doi:10.1029/2010JC006344, 2011.

Van As, D., Andersen, M. L., Petersen, D., Fettweis, X., Van Angelen, J. H., Lenaerts, J. T. M., Van Den Broeke, M. R., Lea, J. M., Bøggild, C. E., Ahlstrøm, A. P., and Steffen, K.: Increasing meltwater discharge from the Nuuk region of the Greenland ice sheet and implications for mass balance (1960–2012), J. Glaciol., 60, 314–322, doi:10.3189/2014JoG13J065, 2014.

Wanninkhof, R.: Relationship between gas exchange and wind speed over the ocean, J. Geophys. Res., 97, 7373–7381, 1992.

Wanninkhof, R. and McGillis, W. R.: A cubic relationship between air–sea CO_2 exchange and wind speed, Geophys. Res. Lett., 26, 1889–1892, doi:10.1029/1999GL900363, 1999.

Whitfield, M. and Turner, D.: The carbon dioxide system in estuaries-an inorganic perspective, Sci. Total Environ., 49, 235–255, available at: http://www.sciencedirect.com/science/article/pii/0048969786902433 (last access: 23 September 2014), 1986.

Wolf-Gladrow, D. A., Zeebe, R. E., Klaas, C., Körtzinger, A., and Dickson, A. G.: Total alkalinity: the explicit conservative expression and its application to biogeochemical processes, Mar. Chem., 106, 287–300, doi:10.1016/j.marchem.2007.01.006, 2007.

BGD
11, 17925–17965, 2014

Table 1. Mass balance equations of the biogeochemical model. V_i and A_i are respectively the volumes and areas of the different zones. ΔpCO_2 is the difference in pCO_2 of the water (modelled) and the atmospheric pCO_2 (400 µatm) with negative values implying an uptake by the sea. α is the CO_2 solubility (mol m^{-3} atm^{-1}). K_{av} (m s^{-1}) is the gas transfer coefficient calculated using the formulation of Nightingale et al. (2000). NCP is the net community production.

Water mass balance		
Zone 1:	$Q_1(t) = Q_2(t) + F_1(t)$	1
Zone 2:	$Q_2(t) = Q_3(t) + F_2(t)$	2
Zone 3:	$Q_3(t) = Q_g(t) + F_3(t)$	3
Salinity mass balance		
Zone 1:	$\frac{dS_1}{dt} = \frac{1}{V_1}(Q_2(t)S_2 + F_1(t)S_{SW} - Q_1(t)S_1)$	4
Zone 2:	$\frac{dS_2}{dt} = \frac{1}{V_2}(Q_3(t)S_3 + F_2(t)S_{SW} - Q_2(t)S_2)$	5
Zone 3:	$\frac{dS_3}{dt} = \frac{1}{V_3}(Q_g(t)S_{FW} + F_3(t)S_{SW} - Q_3(t)S_3)$	6
Total alkalinity (TA) mass balance		
Zone 1:	$\frac{dTA_1}{dt} = \frac{1}{V_1}(Q_2(t)TA_2 + F_1(t)TA_{SW} - Q_1(t)TA_1)$	7
Zone 2:	$\frac{dTA_2}{dt} = \frac{1}{V_2}(Q_3(t)TA_3 + F_2(t)TA_{SW} - Q_2(t)TA_2)$	8
Zone 3:	$\frac{dTA_3}{dt} = \frac{1}{V_3}(Q_g(t)TA_{FW} + F_3(t)TA_{SW} - Q_3(t)TA_3)$	9
Dissolved inorganic carbon (DIC) balance		
Zone 1:	$\frac{dDIC_1}{dt} = \frac{1}{V_1}(Q_2(t)DIC_2 + F_1(t)DIC_{SW} - Q_1(t)DIC_1) - \frac{A_1}{V_1}K_{av}\alpha\Delta pCO_2(t) - NCP_1(t)$	10
Zone 2:	$\frac{dDIC_2}{dt} = \frac{1}{V_2}(Q_3(t)DIC_3 + F_2(t)DIC_{SW} - Q_2(t)DIC_2) - \frac{A_2}{V_2}K_{av}\alpha\Delta pCO_2(t) - NCP_2(t)$	11
Zone 3:	$\frac{dDIC_3}{dt} = \frac{1}{V_3}(Q_g(t)DIC_{FW} + F_3(t)DIC_{SW} - Q_3(t)DIC_3) - \frac{A_3}{V_3}K_{av}\alpha\Delta pCO_2(t) - NCP_3(t)$	12

BGD
11, 17925–17965, 2014

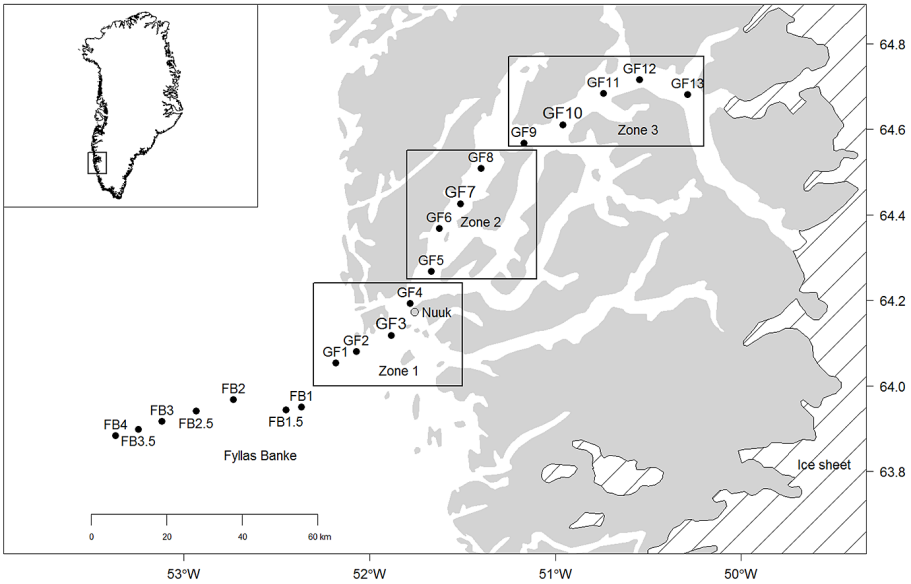

Figure 1. Map of the Godthåbsfjord system with the sampling stations in the fjord system and at Fyllas Banke (SW Greenland). The fjord system is divided in 3 zones indicated by a box. Meteorological data is available from a station in Nuuk.

BGD
11, 17925–17965, 2014

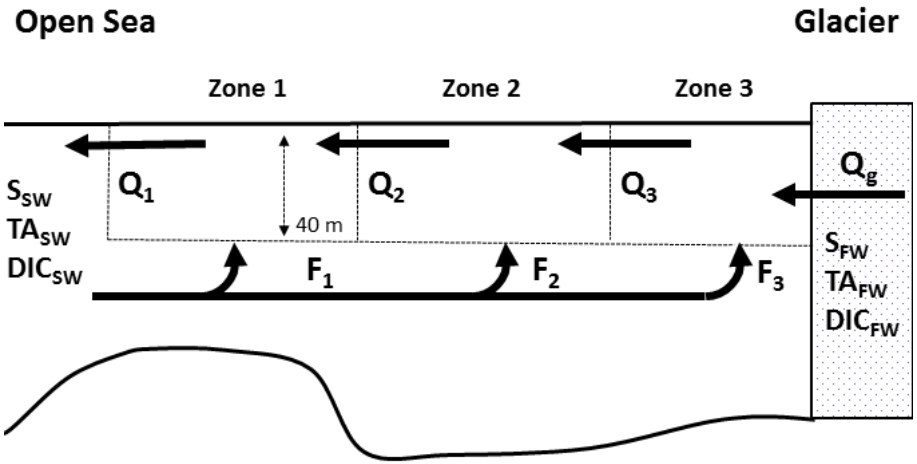

Figure 2. Conceptual model of the fjord system from glacier (right) to open sea (left). The fjord is divided in 3 zones (according to the zones indicated on the overview map).

BGD
11, 17925–17965, 2014

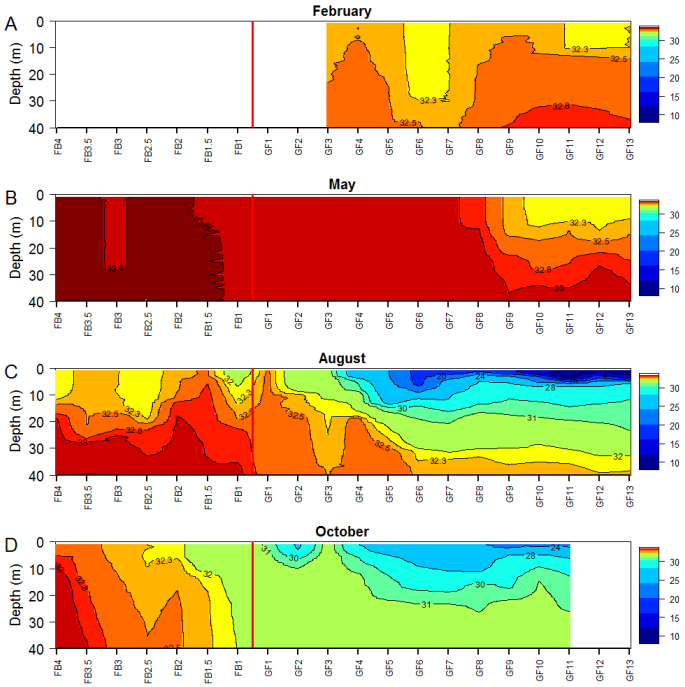

Figure 3. Transects of salinity from shelf (left) to the glaciers (right) during February **(a)**, May **(b)**, August **(c)** and October **(d)** 2013. The red line indicates the mouth of Godthåbsfjord area.

BGD
11, 17925–17965, 2014

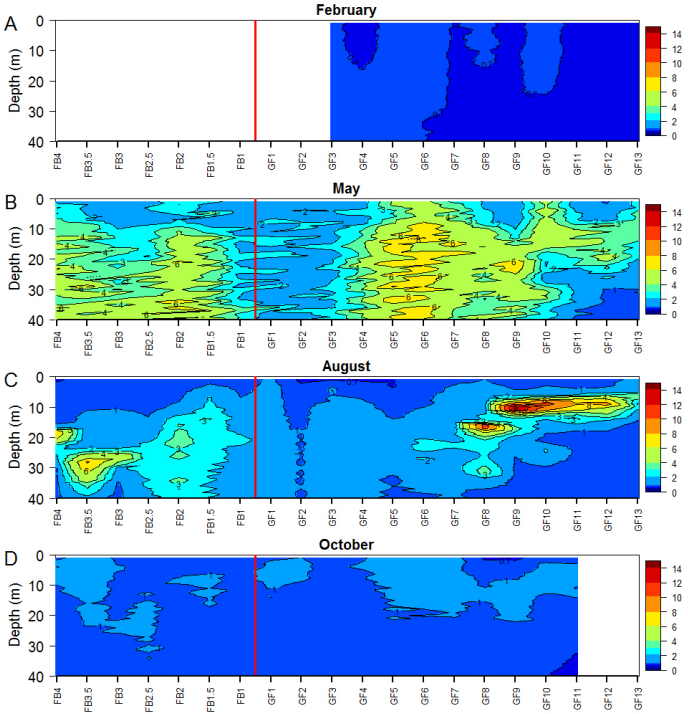

Figure 4. Transects of fluorescence (calibrated vs. chlorophyll *a* in µg L^{-1}) from shelf area (left) to glaciers (right) during February **(a)**, May **(b)**, August **(c)** and October **(d)** 2013. The red line indicates the mouth of Godthåbsfjord area.

BGD
11, 17925–17965, 2014

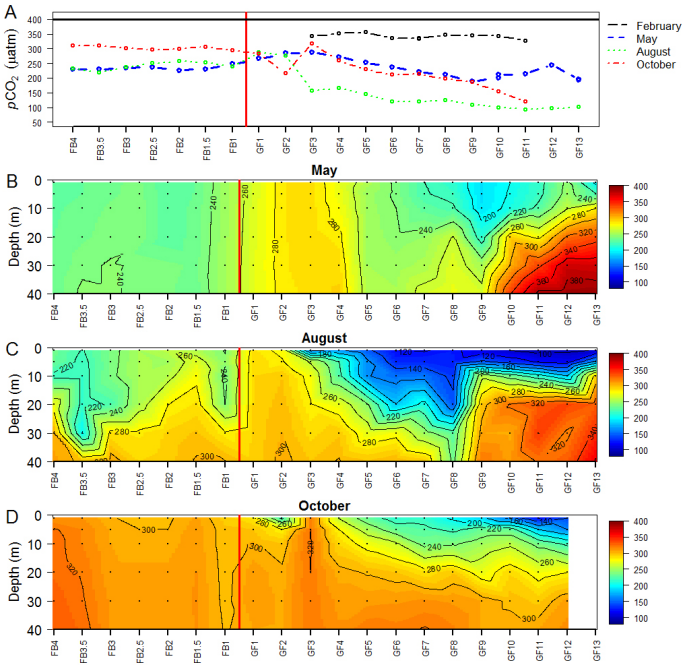

Figure 5. Partial CO_2 pressure data (pCO_2 in µatm) at 1 m depth for the four cruises **(a)**. The full line indicates the average atmospheric concentration (400 µatm) measured during the year 2013. pCO_2 data for the May **(b)**, August **(c)** and October **(d)** cruise in the upper 40 m water column from shelf area (left) to glaciers (right). The red line indicates the mouth of Godthåbsfjord area.

BGD
11, 17925–17965, 2014

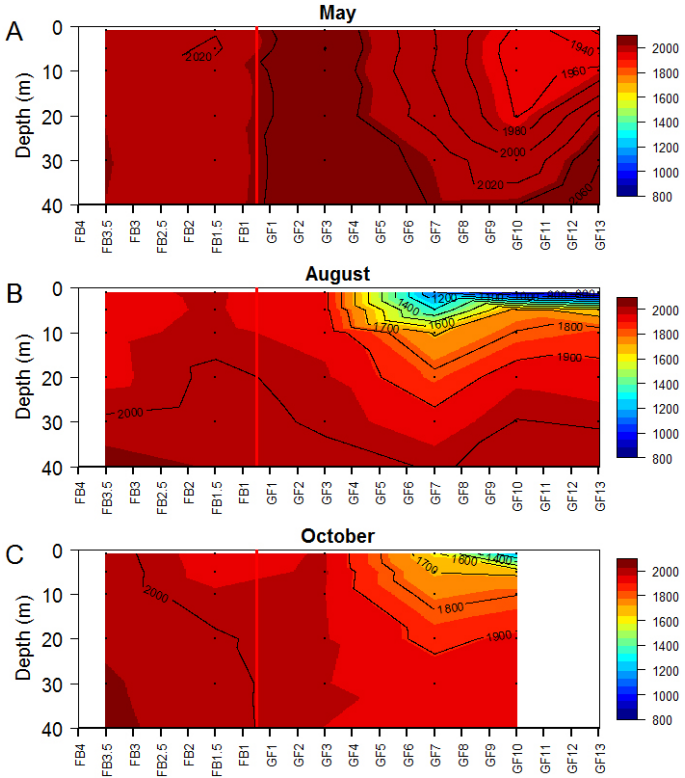

Figure 6. Dissolved inorganic carbon (DIC in $\mu mol\,kg^{-1}$) data for May **(a)**, August **(b)** and October **(c)** 2013 along a transect from the shelf (left) to the glaciers (right). The red line indicates the mouth of Godthåbsfjord area.

BGD
11, 17925–17965, 2014

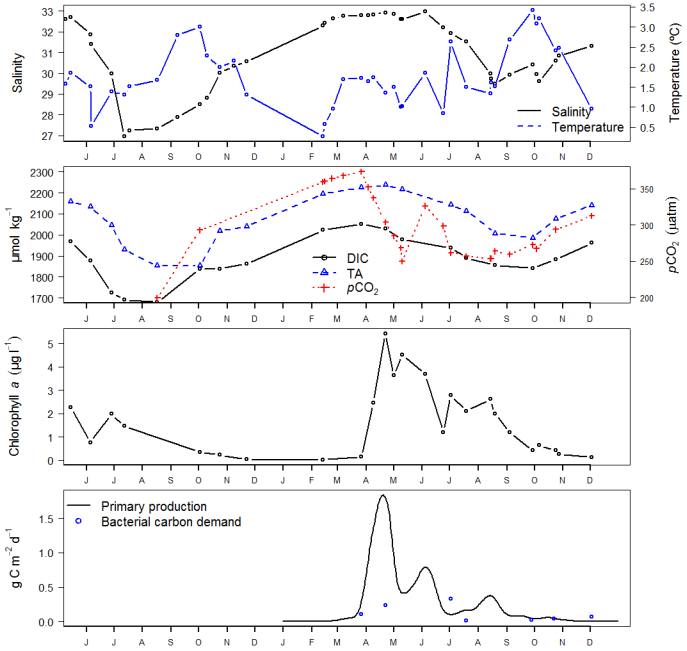

Figure 7. Time series of average (0–40 m) salinity and temperature (°C) **(a)**, DIC, TA (µmol kg^{-1}) and CO_2 partial pressure (pCO_2, µatm) **(b)** chlorophyll *a* concentration (µg L^{-1}) **(c)** and primary production and bacterial carbon demand (g C m^{-2} d^{-1}) **(d)** from June 2012 to December 2013 for station GF10.

BGD
11, 17925–17965, 2014

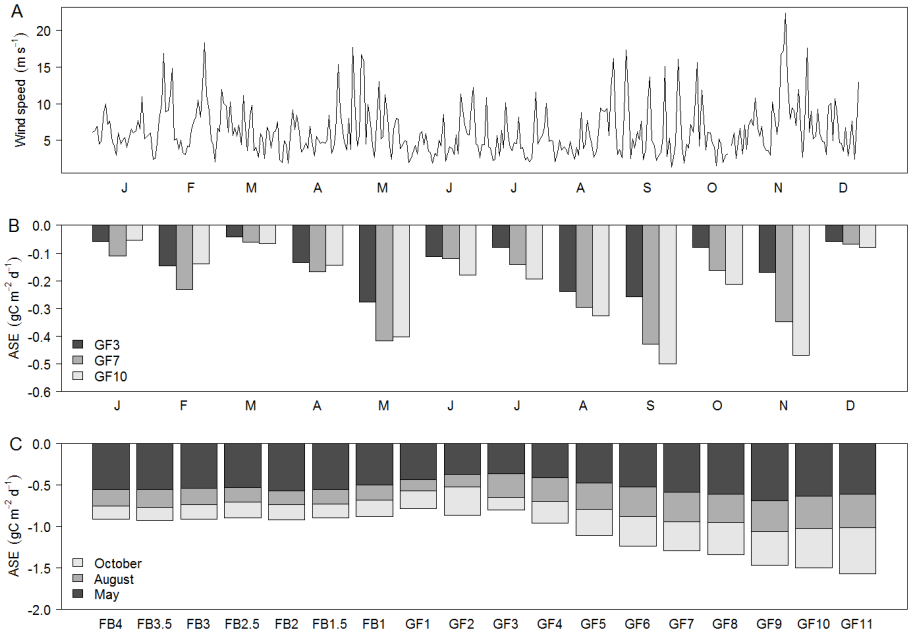

Figure 8. (a) Mean daily wind speed ($m\,s^{-1}$) at the meteorological station in Nuuk. **(b)** Time series of mean monthly air–sea CO_2 flux (ASE, $g\,C\,m^{-2}\,d^{-1}$) at three stations (GF3, GF7 and GF10) in the fjord. **(c)** Mean air–sea exchange (ASE, $g\,C\,m^{-2}\,d^{-1}$) from 3 cruises in fjord system from shelf (Fyllas Banke, left) to inner fjord glaciers (right).

BGD
11, 17925–17965, 2014

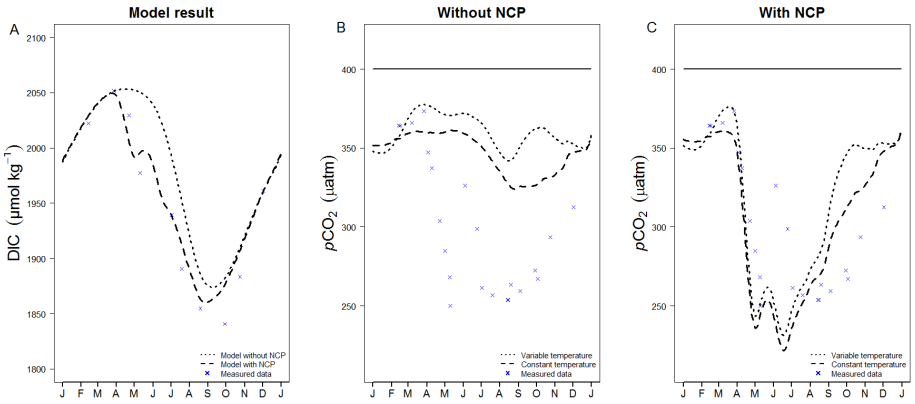

Figure 9. Seasonal evolution of DIC in µmol kg^{-1} **(a)** and pCO_2 in µatm (**b** and **c**) calculated by the biogeochemical model together with data from 2013 in station GF10 (blue points indicate measured data averaged over a 40 m box). Simulations of the model are shown with and without net community production (NCP). Simulations of the evolution of pCO_2 are shown without **(b)** and with NCP **(c)** and for a variable temperature and constant temperature (0.5 °C, the average winter temperature).

BGD
11, 17925–17965, 2014

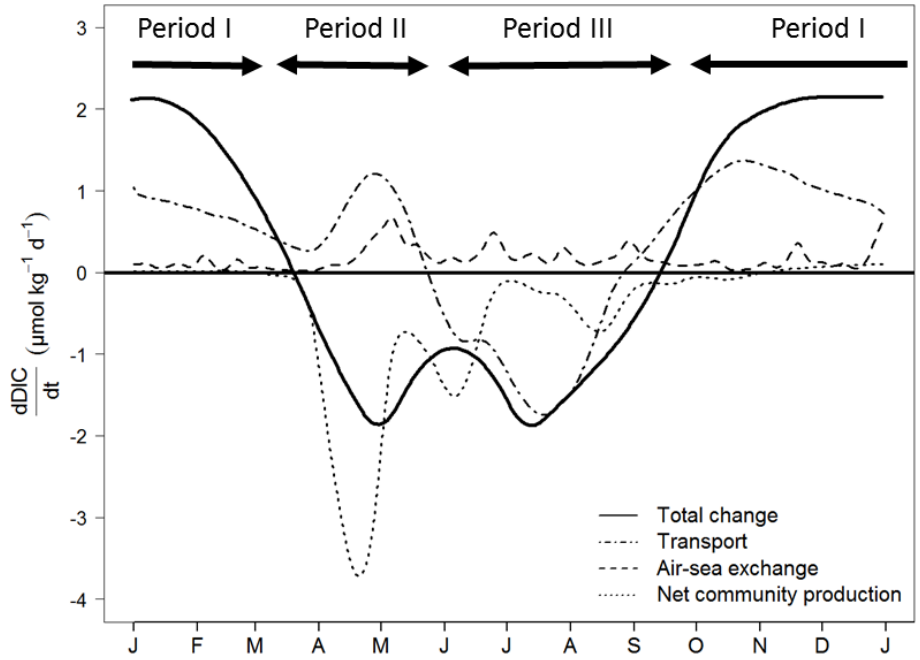

Figure 10. Overview of how different processes (Transport, Air–sea exchange and Net community production) contribute to the temporal observed change in DIC (µmol kg^{-1} d^{-1}) for the station close to the ice sheet (GF10). Uptake of CO_2 by the sea from the atmosphere is shown as a positive value.

BGD
11, 17925–17965, 2014

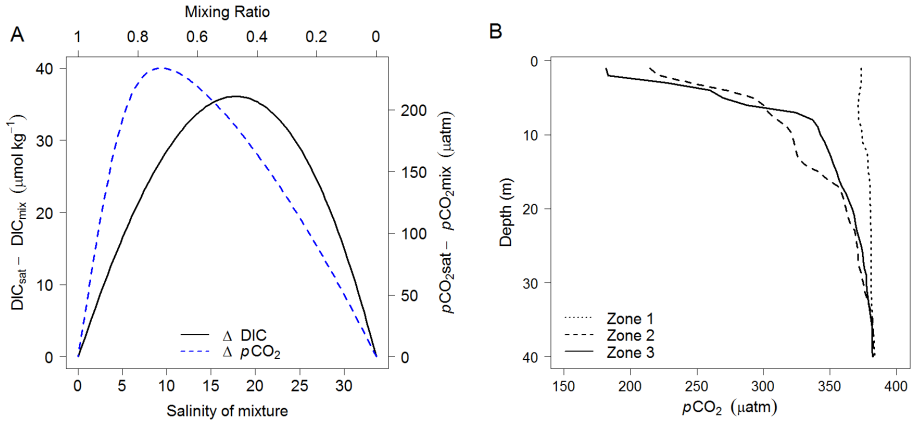

Figure 11. Undersaturation created as ΔDIC (in µmol kg^{-1}) and ΔpCO_2 (in µatm) as a function of salinity of the mixture (and mixing ratio, x, indicating the fraction freshwater) when two water masses in equilibrium with atmosphere are mixed **(a)**. A first water parcel in equilibrium with the atmosphere with TA of 50 µmol kg^{-1}, DIC of 81.2 µmol kg^{-1}, salinity of 0 and temperature of 0 °C (glacial origin). And a second parcel in equilibrium with the atmosphere with TA of 2220 µmol kg^{-1}, DIC of 2118 µmol kg^{-1}, salinity of 33.65 and temperature of 0 °C (fjord/sea water). Panel **(b)** shows the estimated pCO_2 profile calculated from the salinity profiles of August in the three different zones in the fjord system.

BGD
11, 17925–17965, 2014